NeuroImage: Clinical 28 (2020) 102495

Contents lists available at ScienceDirect

NeuroImage: Clinical

journal homepage: www.elsevier.com/locate/ynicl

Multimodal MRI analysis of basal forebrain structure and function across the Alzheimer's disease spectrum

Meret Herdick [a,b], Martin Dyrba [a], Hans-Christian J. Fritz [a,b], Slawek Altenstein [c,d], Tommaso Ballarini [e], Frederic Brosseron [e,f], Katharina Buerger [g,h], Arda Can Cetindag [i], Peter Dechent [j], Laura Dobisch [k], Emrah Duezel [k,l], Birgit Ertl-Wagner [m], Klaus Fliessbach [e,f], Silka Dawn Freiesleben [i], Ingo Frommann [e], Wenzel Glanz [k], John Dylan Haynes [n], Michael T. Heneka [e,f], Daniel Janowitz [h], Ingo Kilimann [a,b], Christoph Laske [o,p], Coraline D. Metzger [k,l,q], Matthias H. Munk [o,p], Oliver Peters [c,i], Josef Priller [c,d], Nina Roy [e], Klaus Scheffler [r], Anja Schneider [e,f], Annika Spottke [e,s], Eike Jakob Spruth [c,d], Maike Tscheuschler [t], Ruth Vukovich [u], Jens Wiltfang [u,v,w], Frank Jessen [e,t,x], Stefan Teipel [a,b,*], Michel J. Grothe [a,y,*]

[a] German Center for Neurodegenerative Diseases (DZNE), Rostock, Germany
[b] Department of Psychosomatic Medicine, Rostock University Medical Center, Rostock, Germany
[c] German Center for Neurodegenerative Diseases (DZNE), Berlin, Germany
[d] Department of Psychiatry and Psychotherapy, Charité, Charitéplatz 1, 10117 Berlin, Germany
[e] German Center for Neurodegenerative Diseases (DZNE), Bonn, Venusberg-Campus 1, 53127 Bonn, Germany
[f] Department for Neurodegenerative Diseases and Geriatric Psychiatry, University Hospital Bonn, Venusberg-Campus 1, 53127 Bonn, Germany
[g] German Center for Neurodegenerative Diseases (DZNE, Munich), Feodor-Lynen-Strasse 17, 81377 Munich, Germany
[h] Institute for Stroke and Dementia Research (ISD), University Hospital, LMU Munich, Feodor-Lynen-Strasse 17, 81377 Munich, Germany
[i] Charité – Universitätsmedizin Berlin, Corporate Member of Freie Universität Berlin, Humboldt-Universität zu Berlin, and Berlin Institute of Health, Institute of Psychiatry and Psychotherapy, Hindenburgdamm 30, 12203 Berlin, Germany
[j] MR-Research in Neurology and Psychiatry, Georg-August-University Göttingen, Germany
[k] German Center for Neurodegenerative Diseases (DZNE), Magdeburg, Germany
[l] Institute of Cognitive Neurology and Dementia Research (IKND), Otto-von-Guericke University, Magdeburg, Germany
[m] Institute for Clinical Radiology, Ludwig-Maximilians-University, Marchioninistr. 15, 81377 Munich, Germany
[n] Bernstein Center for Computational Neuroscience, Charité — Universitätsmedizin, Berlin, Germany
[o] German Center for Neurodegenerative Diseases (DZNE), Tübingen, Germany
[p] Section for Dementia Research, Hertie Institute for Clinical Brain Research and Department of Psychiatry and Psychotherapy, University of Tübingen, Tübingen, Germany
[q] Department of Psychiatry and Psychotherapy, Otto-von-Guericke University, Magdeburg, Germany
[r] Department for Biomedical Magnetic Resonance, University of Tübingen, 72076 Tübingen, Germany
[s] Department of Neurology, University of Bonn, Venusberg-Campus 1, 53127 Bonn, Germany
[t] Department of Psychiatry, University of Cologne, Medical Faculty, Kerpener Strasse 62, 50924 Cologne, Germany
[u] Department of Psychiatry and Psychotherapy, University Medical Center Goettingen, University of Goettingen, Von-Siebold-Str. 5, 37075 Goettingen, Germany
[v] German Center for Neurodegenerative Diseases (DZNE), Goettingen, Germany
[w] Neurosciences and Signaling Group, Institute of Biomedicine (iBiMED), Department of Medical Sciences, University of Aveiro, Aveiro, Portugal
[x] Excellence Cluster on Cellular Stress Responses in Aging-Associated Diseases (CECAD), University of Cologne, Joseph-Stelzmann-Strasse 26, 50931Köln, Germany
[y] Unidad de Trastornos del Movimiento, Servicio de Neurología y Neurofisiología Clínica, Instituto de Biomedicina de Sevilla, Hospital Universitario Virgen del Rocío/CSIC/Universidad de Sevilla, Seville, Spain

ARTICLE INFO

ABSTRACT

Abbreviations: AD, Alzheimer's Disease; cBF, cholinergic basal forebrain; dACC, dorsal anterior cingulate; DTI, diffusion tensor imaging; FC, functional connectivity; GM, gray matter; MCI, mild cognitive impairment; MD, mean diffusity; NBM, nucleus basilis of Meynert; SCD, subjective cognitive decline; WM, white matter.

* Corresponding authors at: DZNE German Center for Neurodegenerative Diseases, Rostock, c/o Zentrum für Nervenheilkunde, Gehlsheimer Str. 20, D-18147 Rostock, Germany.

E-mail addresses: stefan.teipel@med.uni-rostock.de (S. Teipel), michel.grothe@dzne.de (M.J. Grothe).

https://doi.org/10.1016/j.nicl.2020.102495
Received 3 August 2020; Received in revised form 19 October 2020; Accepted 2 November 2020
Available online 11 November 2020

Keywords:
Cholinergic Basal Forebrain
Subjective Cognitive Decline
Alzheimer's Disease
Functional Connectivity
Mean Diffusivity
Resting-state fMRI

Background: Dysfunction of the cholinergic basal forebrain (cBF) is associated with cognitive decline in Alzheimer's disease (AD). Multimodal MRI allows for the investigation of cBF changes in-vivo. In this study we assessed alterations in cBF functional connectivity (FC), mean diffusivity (MD), and volume across the spectrum of AD. We further assessed effects of amyloid pathology on these changes.
Methods: Participants included healthy controls, and subjects with subjective cognitive decline (SCD), mild cognitive impairment (MCI), or AD dementia (ADD) from the multicenter DELCODE study. Resting-state functional MRI (rs-fMRI) and structural MRI data was available for 477 subjects, and a subset of 243 subjects also had DTI data available. Differences between diagnostic groups were investigated using seed-based FC, volumetric, and MD analyses of functionally defined anterior (a-cBF) and posterior (p-cBF) subdivisions of a cytoarchitectonic cBF region-of-interest. In complementary analyses groups were stratified according to amyloid status based on CSF Aβ42/40 biomarker data, which was available in a subset of participants.
Results: a-cBF and p-cBF subdivisions showed regional FC profiles that were highly consistent with previously reported patterns, but there were only minimal differences between diagnostic groups. Compared to controls, cBF volumes and MD were significantly different in MCI and ADD but not in SCD. The Aβ42/40 stratified analyses largely matched these results.
Conclusions: We reproduced subregion-specific FC profiles of the cBF in a clinical sample spanning the AD spectrum. At least in this multicentric cohort study, cBF-FC did not show marked changes along the AD spectrum, and multimodal MRI did not provide more sensitive measures of AD-related cBF changes compared to volumetry.

1. Introduction

The cholinergic basal forebrain (cBF) provides the principle cholinergic innervation of the entire cerebral cortex (Mesulam et al., 1983). It has become an important region of interest for research on Alzheimer's disease (AD) since neuropathological studies have documented selective cBF neuron loss in AD dementia (ADD) (McGeer et al., 1984; Whitehouse et al., 1982, 1981). The prominent role of cBF degeneration in AD has led to the development of cholinomimetic drugs for dementia treatment.

Advances in regional volumetric analysis allowed for the development of an MRI-based in-vivo marker of cBF degeneration showing early degeneration of this region within the AD spectrum (Grothe et al., 2012; Kilimann et al., 2014). Further studies suggested that in preclinical and prodromal stages of AD, cBF volume may be even more sensitive to early degenerative changes than hippocampal or entorhinal cortex atrophy (Kilimann et al., 2014; Schmitz et al., 2016). In vivo MRI-PET studies and a recent imaging-neuropathological association study suggest that cBF atrophy may be associated with cortical amyloid pathology in prodromal and dementia stages of AD (Grothe et al., 2014; Kerbler et al., 2015; Teipel et al., 2020).

Beyond volumetric changes, previous MRI studies also reported microstructural changes of the cBF in AD as measured by diffusion tensor imaging (DTI) (Brueggen et al., 2015; Teipel et al., 2011), which sensitizes the MRI signal to the movement of hydrogen (Basser et al., 1994; Uluğ et al., 1999). In damaged neuronal tissue, the amount of cellular water diffusion is changed, which can be detected by DTI-derived scalar diffusion indices, such as mean diffusivity (MD), even before macrostructural (volumetric) degeneration becomes visible (Teipel et al., 2014b). We piloted DTI assessment of the cBF in a multicenter cohort of subjects with mild cognitive impairment (MCI) and ADD, and results indicated a higher risk of conversion to dementia in MCI patients with increased MD (Brueggen et al., 2015). Previous studies showed increased MD levels across the spectrum of AD in hippocampal structures (Hong et al., 2012; Müller et al., 2007; Ryu et al., 2017), and an investigation in Parkinson's disease patients suggested that diffusion changes in the nucleus basalis of Meynert may be sensitive to very early stages of neurodegeneration (Schulz et al., 2018).

Another potentially powerful approach to determine cBF changes uses functional connectivity (FC) from resting state functional magnetic resonance imaging (rs-fMRI). Rs-fMRI is based on the measurement of spontaneous fluctuations of the BOLD (blood oxygen level dependent) signal, which reflects activity-dependent changes in blood oxygenation in the brain (Biswal et al., 1995; Glover, 2011). In AD, rs-fMRI has so far mainly been used for studying AD-related neurodegenerative changes in the hippocampus and the default mode network (Wang et al., 2006; Zhang et al., 2009; Zhou et al., 2008). In a recent methodological study based on a sample of healthy adult individuals, we were able to demonstrate the feasibility of measuring cortical FC profiles of the cBF based on rs-fMRI data and could identify two functionally distinct anterior-medial and posterior-lateral subdivisions of the cBF based on their differential cortical connectivity profiles (Fritz et al., 2019).

In the present study we evaluated comprehensive volumetric, microstructural and FC changes of the cBF in a large clinical sample spanning the cognitive spectrum from normal cognition through subjective cognitive decline (SCD) and MCI to ADD. In a subsample with available cerebrospinal fluid (CSF) biomarker data, we further stratified diagnostic groups by amyloid status. We expected to detect robust changes in cBF volume only in prodromal and dementia stages of AD, whereas DTI- and rs-fMRI-assessments may already show alterations in preclinical stages of AD.

2. Methods

2.1. Data source

All data used in this study was obtained from the DZNE- Longitudinal Cognitive Impairment and Dementia Study (DELCODE) (Jessen et al., 2018). DELCODE is a German multicenter observational study on predementia AD that aims to characterize early disease stages, in particular SCD, improve disease progression prognostics and identify new markers for preclinical AD (https://www.dzne.de/forschung/studien/klinische-studien/delcode/). DELCODE is an ongoing study that was launched in 2015.

2.2. Subjects

Data for a total of 510 subjects was obtained from an interim freeze of the DELCODE database based on the availability of rs-fMRI scans and the absence of anomalies such as stroke residues or tumors during a visual sighting of structural MRI scans.

Participants had been subdivided into the following groups upon inclusion into the study:

(i) Participants with SCD that were defined by subjectively reported cognitive decline over a period of at least six months not related to any event or condition explaining the cognitive deficit according to research criteria and had an objective test performance within −1.5 standard deviations of the age-, sex-, and education-adjusted normal performance on all subtests of the CERAD (Consortium to Establish a Registry for Alzheimer's Disease) neuropsychological test battery (Jessen et al., 2014).

(ii) MCI and ADD patients who were enrolled based on clinical criteria in accordance with current guidelines by the National Institute

on Aging-Alzheimer's Association (NIA-AA) (Albert et al., 2011; McKhann et al., 2011).

(iii) Healthy controls (HC), who reported no signs of SCD and had to achieve unimpaired test results according to the same definition as the SCD group.

All participants were above the age of 60 years. Exclusion criteria have been described in detail previously (Jessen et al., 2018) and included both drugs and medical conditions that have the potential of interfering with test performance.

During preprocessing of rs-fMRI scans (see below) only subjects with head motion<2 mm translation and 2°rotation were included (N = 477) (Fritz et al., 2019). The final sample for rs-fMRI and volumetric analysis was composed of 174 HC, 171 participants with SCD, 81 MCI subjects, and 51 subjects with ADD. A subset of 281 participants also had DTI scans available, and 243 of these met quality control criteria for the DTI data (see below), resulting in a group of 88 HC, 88 participants with SCD, 40 MCI subjects, and 27 subjects with ADD. Demographics of the subjects that were analysed in this study are shown in Tables 1 and 2.

Written informed consent was provided by all participants or by their representatives prior to inclusion in the study. The study was approved by local ethics committees at each of the participating centers and has been conducted in accordance with the Helsinki Declaration of 1975.

2.3. Cerebrospinal fluid biomarkers

A subset of participants had consented to undergo a lumbar puncture performed by a medically trained study assistant prior to the procedure. CSF measurement was available for a subset of 218 participants in the rs-fMRI sample and 114 participants in the DTI subcohort.

Subjects' amyloid beta 1–42 (Aβ42) and 1–40 (Aβ40) concentrations were determined using commercially available kits (V-PLEX Aβ Peptide Panel 1 (6E10) Kit; Mesoscale Diagnostics LLC, Rockville, USA) according to the vendor's specifications which were centrally processed at the DZNE Biorepository Bonn. Participants with available CSF data were grouped into amyloid positive and negative groups based on a previously established cut-off for the Aβ42/40 ratio (Aβ+: Aβ42/40 ratio < 0.09 (Janelidze et al., 2016)). The resulting sample sizes per diagnostic category are listed in Tables 1 and 2. The amyloid negative HC group as well as all amyloid positive subgroups were used for further analyses.

2.4. Imaging data acquisition

DELCODE MRI data were acquired on nine Siemens MRI scanners including three TIM systems, four Verio systems, one Skyra system, and one Prisma system. Particular emphasis was placed on steps to assure quality and assessment standards across the multicentric acquisitions including unified scanning protocols and standard operating procedures that have been described in detail previously (Jessen et al., 2018).

Table 1
Demographic characteristics of diagnostic groups.

	HC (n = 174)	SCD (n = 171)	MCI (n = 81)	ADD (n = 51)
Amyloid Status (+/-/n.a.)	22/44/108	30/44/97	31/19/31	25/3/23
Gender (m/f)[1]	71/103	91/80	49/32	22/29
Age (SD)[2]	68.9 (5.2)	71.3 (5.9)	72.3 (5.2)	73.0 (6.6)
Education Years (SD)[3]	14.8 (2.7)	14.9 (3.0)	13.9 (3.0)	13.7 (3.1)
MMSE[4]	29.4 (0.9)	29.2 (1.0)	28.0 (1.7)	23.5 (3.5)
GDS[5]	0.6 (1.1)	1.9 (1.9)	2.1 (2.0)	2.0 (1.6)

MMSE, Mini Mental State Examination; GDS, Geriatric Depression Scale. n.a., not available.
[1] Significantly different between groups, $x^2 = 10.9$, df = 3, p = 0.012. [2] Significantly different between groups, Welch's F (3, 166.9) = 11.70, p < 0.001. [3] Significantly different between groups, F (3, 473) = 4.23, p = 0.006. [4] Significantly different between groups, Welch's F (3, 147.1) = 62.2, p < 0.001.[5] Significantly different between groups, Welch's F (3, 151.9) = 31.618, p < 0.001.

Table 2
Demographic characteristics of diagnostic groups in DTI subsample.

	HC (n = 88)	SCD (n = 88)	MCI (n = 40)	ADD (n = 27)
Amyloid Status (+/-/n.a.)	16/18/54	20/19/49	21/7/12	4/9/14
Gender (m/f)[1]	52/36	43/45	13/27	17/10
Age (SD)[2]	68.5 (5.1)	71.5 (5.6)	72.3 (5.9)	72.4 (5.8)
Education Years (SD)[3]	15.2 (2.6)	14.7 (3.1)	14.2 (3.0)	13.5 (2.7)
MMSE[4]	29.5 (0.8)	29.3 (0.9)	27.9 (1.6)	23.1 (3.4)
GDS[5]	0.7 (1.5)	1.8 (1.5)	1.8 (2.0)	1.8 (1.6)

MMSE, Mini Mental State Examination; GDS, Geriatric Depression Scale. n.a., not available.
[1] Significantly different between groups, $x^2 = 9.5$, df = 3, p = 0.024. [2]Significantly different between groups, F (3, 239) = 7.1, p < 0.001. [3]Significantly different between groups, F (3, 239) = 2.7, p = 0.044. [4] Significantly different between groups, Welch's F (3, 74.4) = 41.8, p < 0.001 .[5] Significantly different between groups, F (3, 231) = 8.5, p < 0.001.

Rs-fMRI data was obtained using an echo-planar imaging (EPI) sequence with a 64 · 64 image matrix with 47 axial slices (thickness 3.5 mm, no gap) and interleaved acquisition. The field of view (FOV) was set to 224 · 224 · 165 mm, isotropic voxel size of 3.5 mm, echo time 30 ms, repetition time 2,580 ms, flip angle 80°, and parallel imaging acceleration factor 2.

Diffusion weighted imaging data was obtained using an EPI multishell-sequence with a matrix size of 120 · 120, number of slices 72, a FOV of 240 · 240 mm, isotropic voxel size 2 mm, an echo time of 88 ms, repetition time 12,100 ms, flip angle 90°, 60 gradients at 700 s/mm2 and 1000 s/mm2, and parallel imaging acceleration factor 2.

Additionally, high-resolution structural MRI images were recorded and used both as anatomical references for image preprocessing of rs-fMRI and DTI data as well as for the analysis of volumetric changes. Structural MRIs were based on a T1-weighted magnetization-prepared rapid gradient echo (MPRAGE) sequence with the following parameters: 256 · 256 image matrix with 192 sagittal slices; FOV: 250 · 250 · 192 mm; 1 mm isotropic voxel size; 4.37 ms echo time; 2500 ms repetition time; 7° flip angle; and parallel imaging acceleration factor 2.

Rs-fMRI and structural MRI images were recorded in the same session. The DTI scans were recorded on the same day or an optional second day of scanning (average difference in days: 6 ± 14).

2.5. Cholinergic basal forebrain regions of interest

The cBF regions of interest (ROIs) that were examined in this study were based on our previous methodological work characterizing functionally homogeneous subdivisions within a stereotactic atlas of the cBF using a data-driven clustering analysis of voxel-wise cBF FC profiles in a healthy adult population (Fritz et al., 2019). The two resulting subdivisions consisted of an anterior-medial (a-cBF) and a posterior-lateral (p-cBF) subdivision of the cBF (Fig. 1**A**). When compared to cytoarchitectonically defined cBF subdivisions, the a-cBF largely corresponds to the rostral nuclei of the medial septum/diagonal band and anterior medial parts of the Nucleus basalis of Meynert (NBM), whereas the p-cBF covers the remaining anterior-lateral, intermediate, and posterior parts of the NBM.

2.6. Imaging data processing and statistical analysis

2.6.1. Structural MRI data

For structural MRI segmentation into gray matter (GM), white matter (WM), and CSF partitions and normalization to the Montreal Neurological Institute (MNI) reference space applying the Diffeomorphic Anatomical Registration Through Exponentiated Lie Algebra (DARTEL)

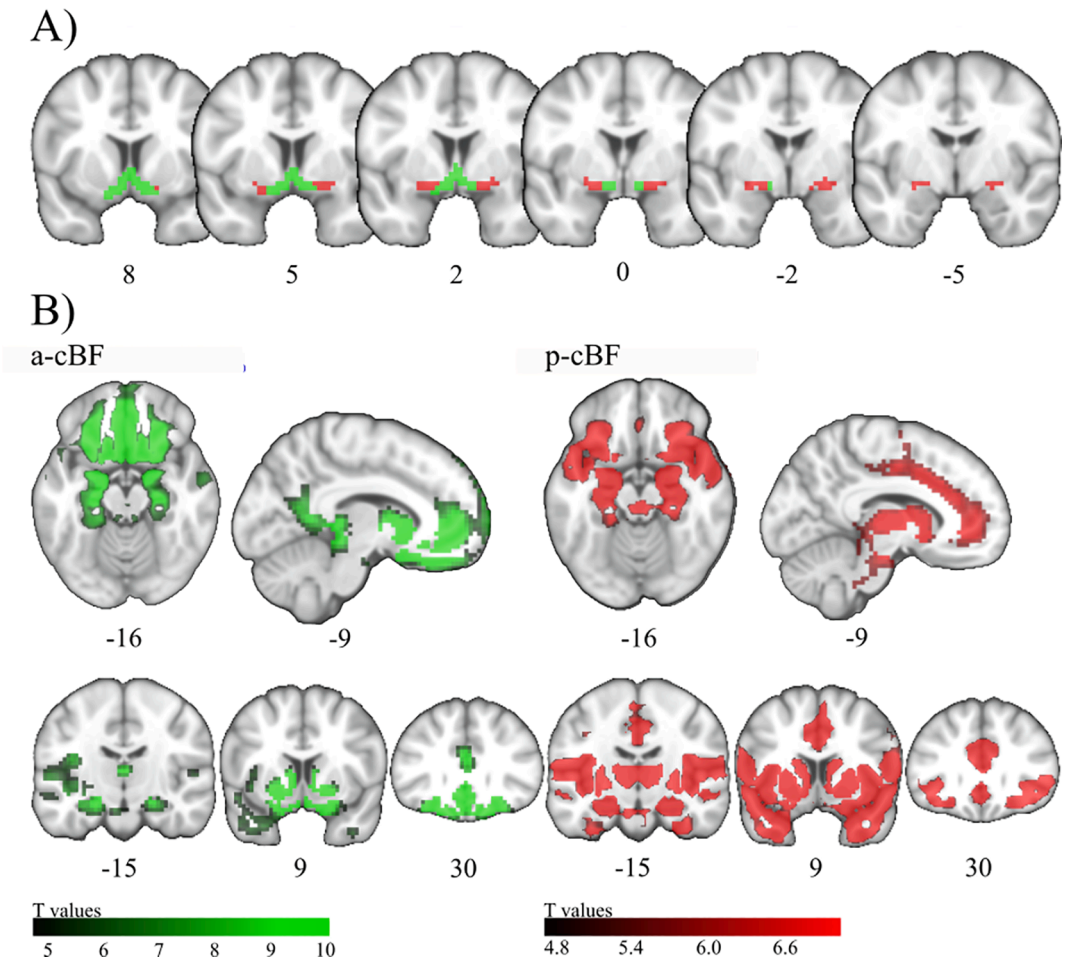

Fig. 1. Anatomic location and functional connectivity profiles of the cBF. A) Coronal slices from anterior to posterior showing the anterior-medial (a-cBF, green) and posterior-lateral (p-cBF, red) cBF regions of interest on representative coronal sections. B) Functional connectivity across all groups for a-cBF and p-cBF regions of interest on representative axial, mid-sagittal, and three coronal sections. Numbers below the brain sections indicate Montreal Neurological Institute (MNI) standard space coordinates. Colorbar indicates T-values ($p < 0.05$ [FWE]). (For interpretation of the references to colour in this figure legend, the reader is referred to the web version of this article.)

algorithm (Ashburner, 2007) the Computational Anatomy Toolbox 12 (CAT12, http://dbm.neuro.uni-jena.de/cat/) of SPM12 was used. Deformation-fields resulting from this registration were used to warp the GM segments, including modulation of voxel values in order to preserve the total amount of GM volume present before warping. Individual GM volumes of the cBF ROIs were extracted from the preprocessed GM segments by summing up the modulated GM voxel values within the respective ROI masks. cBF volumes were divided by the total intracranial volume (TIV) that was calculated as the total sum of GM, WM, and CSF volumes.

2.6.2. rs-fMRI data

For preprocessing of fMRI data, we used the advanced version of the Data Processing Assistant for rs-fMRI (DPARSF, Version 2.2, State Key Laboratory of Cognitive Neuroscience and Learning, Beijing Normal University, Beijing, China) (Yan and Zang, 2010) running under Statistical Parametric Mapping software (SPM12; Wellcome Dept. of Imaging Neuroscience, London) implemented in MATLAB 7.1 (Mathworks, Natwick). The initial ten time points of the rs-fMRI series were discarded, and the remaining images were slice time corrected. The images were realigned and thereafter checked for head motion of>2 mm and 2° in maximum head motion, which were consequently excluded (N = 35) (Fritz et al., 2019). Every participant's T1-weighted image was coregistered to the mean functional image. Subsequently, nuisance covariates were regressed out using 24 head motion parameters (Friston et al., 1996) as well as WM and CSF signal as nuisance regressors, including a linear detrend. In a next step, the rs-fMRI images were band pass filtered to 0.01 and 0.1 Hz, spatially normalized to MNI space using the deformation fields derived from the co-registered T1-weighted MRI scan, resliced to an isotropic voxel resolution of 3 mm, and smoothed with a 6 mm full width at half maximum (FWHM) Gaussian kernel. For seed-based FC analysis, a-cBF and p-cBF ROIs were defined as seeds and FC was calculated based on the Pearson correlation coefficient of the seeds' and each other voxels' time series (Joel et al., 2011). The resulting voxel-wise FC maps were Fisher z-transformed for further statistical analysis.

2.6.3. DTI data

Diffusion-weighted images were preprocessed using the diffusion toolbox in the FMRIB Software Library (FSL, Version 5.0.4, Oxford Center for Functional MRI of the Brain, Oxford, UK). First, scans were corrected for eddy currents and head motion. Skull stripping was performed using the Brain Extraction Tool and diffusion tensors were fitted to the data by applying DTIfit yielding the MD maps. Next, the B0 images were co-registered to the corresponding T1-weighted MRIs and the same transformations were applied to the MD maps. The MD maps were spatially normalized to MNI-standard space by applying the deformation field from the co-registered T1-weighted MRI (without modulation). Regional MD of the a-cBF and p-cBF ROIs were then calculated by averaging the respective voxel intensities in the spatially normalized MD

maps.

2.6.4. Statistical analysis

Statistical analysis of ROI values in volume and MD analyses was performed using the statistics software package for the social sciences (SPSS, IBM Corp. Version 25.0.). The effect of diagnosis on a-cBF and p-cBF volumes and MD values was assessed using ANCOVA, with age, gender, education years, and acquisition site as covariates. Note that accounting for "acquisition site" in the model entails control for differences in scanner models but also other potential differences across sites. In order to evaluate differences in the estimated marginal means, pairwise post-hoc t-tests of the diagnosis-specific contrasts were performed. All tests were two-tailed and statistical significance was set to $p < 0.05$. Cohen's d effect sizes of the group differences were calculated based on the adjusted group means.

Statistical analysis of FC differences was performed using SPM12. First, overall FC profiles of the a-cBF and p-cBF seeds were calculated using a second-level one-sample *t*-test of all subjects' FC maps, controlled for acquisition site, age, years of education, and gender. FC maps were restricted to the brain's GM, thresholded at $p < 0.05$ corrected for multiple testing by employing the Family-wise error rate (FWE), and binarized to yield masks for the analysis of FC group differences.

To determine significant changes in FC between HC and the other diagnostic groups, a series of voxel-wise two-sample t-tests were performed on the FC maps, controlled for acquisition site, age, years of education, and gender. The analyses were restricted to the seed region-specific FC masks that were calculated in the previous step, and voxel-wise results were transformed to Cohen's d maps thresholded at $p < 0.001$, uncorrected for multiple comparisons, with an additional cluster-size threshold of $k > 10$ voxels (270 mm^3).

In complementary analyses in subjects with available CSF measures, all voxel- and ROI-wise statistical analyses of group differences were repeated in amyloid stratified groups. Specifically, the following contrasts were considered: HC^- vs HC^+, HC^- vs SCD^+, HC^- vs MCI^+, HC^- vs ADD^+.

3. Results

3.1. Demographics

Demographics of the study sample by diagnostic group are presented in Tables 1 and 2. In the full study sample, all patient groups differed significantly from the HC group with respect to age ($p < 0.001$), with controls being on average 2.4 years younger than SCD, 3.4 years younger than MCI and 4.1 years younger than ADD participants. The education level also differed significantly across diagnostic groups ($p = 0.006$), with the HC and SCD groups having on average one year more of formal education than the MCI and ADD groups. The sex distribution of SCD ($p = 0.021$) and MCI ($p = 0.003$) participants differed significantly from HC.

3.2. FC analysis

3.2.1. cBF functional connectivity profiles

FC profiles of the a-cBF and p-cBF subdivisions across all diagnostic groups showed specific patterns of connectivity with distributed cortical systems (Fig. 1**B**). The a-cBF profile was characterised by prominent connectivity to the retrosplenial/posterior cingulate cortex and the ventromedial prefrontal cortex. The p-cBF profile was distinguished by predominant FC with the insula, dorsal anterior cingulate (dACC), and the thalamus. Areas of overlapping connectivity of a-cBF and p-cBF seeds were seen in the posterior ventromedial prefrontal cortex, the temporal pole, and the medial temporal lobe.

3.2.2. Between group differences in cBF functional connectivity

When compared to the HC group, FC of the a-cBF did not differ significantly in SCD, whereas the MCI group showed a small cluster of 18 voxels with reduced connectivity in the medial part of the right superior frontal gyrus, and the ADD group showed a larger cluster (74 voxels) of reduced connectivity in the left and right anterior cingulate and the medial part of the right superior frontal gyrus (Fig. 2).

For the p-cBF, no significant differences in FC were observed between the SCD and HC group. The MCI group showed two small clusters of reduced connectivity in the right midcingulate area (13 voxels) and the right superior temporal area (23 voxels). The ADD subjects showed reduced connectivity in two small clusters in the left anterior cingulate region (23 voxels) and the right parahippocampal region (18 voxels) (Fig. 3).

3.3. cBF volume

There was a significant overall effect of diagnosis on both a-cBF ($F = 12.05$, $p < 0.001$) and p-cBF ($F = 14.19$, $p < 0.001$) volume (Fig. 4**A**). Compared to HC, a-cBF volume was significantly smaller in MCI (-5.1 percent, $p < 0.001$; Cohen's $d = -0.52$) and ADD patients (-11 percent, $p < 0.001$; Cohen's $d = -1.12$), but was not significantly different in the SCD group (+0.1 percent, $p = 0.90$; Cohen's $d = 0.01$). Similarly, p-cBF volume was significantly smaller in MCI (-5.9 percent, $p < 0.001$; Cohen's $d = -0.60$) and ADD patients (-14.7 percent, $p < 0.001$; Cohen's $d = -1.48$) as compared to the HC group, but was not significantly different in the SCD group (-0.3 percent, $p = 0.89$; Cohen's $d = -0.03$).

3.4. cBF MD

There was a significant overall effect of diagnosis on both a-cBF ($F = 9.28$, $p < 0.001$) and p-cBF ($F = 4.03$; $p = 0.008$) MD values (Fig. 4**B**). In both cBF areas the mean MD rose continuously from the HC to the SCD, MCI, and ADD groups. Compared to HC, a-cBF MD was significantly higher in MCI (+14.7 percent, $p = 0.001$; Cohen's $d = 0.69$) and ADD patients (+22.1 percent, $p < 0.001$; Cohen's $d = 1.03$), but was not significantly different in the SCD group (+5.0 percent, $p = 0.13$; Cohen's $d = 0.24$). The p-cBF MD was significantly higher in MCI (+9.3 percent,

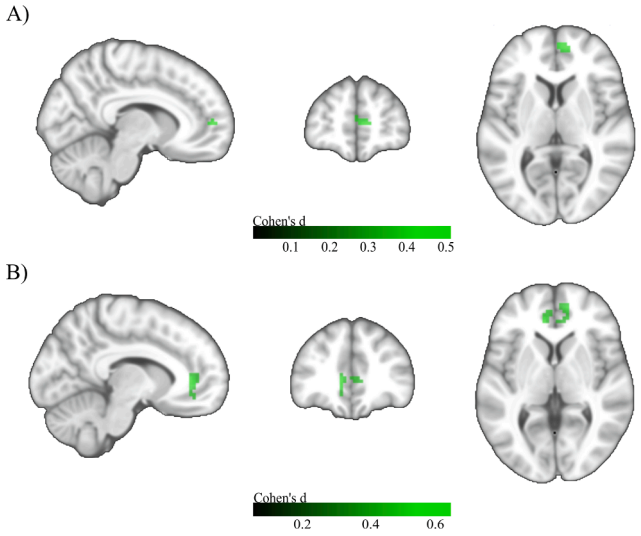

Fig. 2. Voxel-wise group differences in a-cBF functional connectivity. A) Group differences between HC and MCI. MNI coordinates: X = 9, Y = 54, Z = 6. B) Group differences between HC and ADD. MNI coordinates: X = -9, Y = 39, Z = 3. Two sample t-tests controlled for age, gender, years of education, and acquisition site. Colorbar indicates Cohen's d effect size values. Results are shown at an uncorrected voxel-wise threshold of $p < 0.001$ with a cluster-size threshold of $k > 10$ voxels.

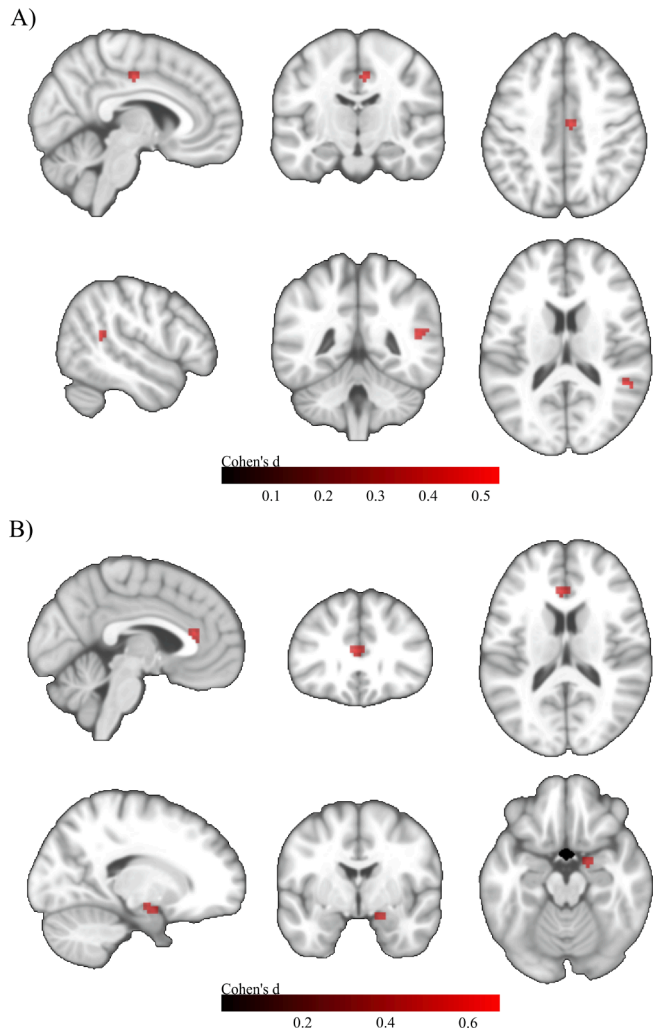

Fig. 3. Voxel-wise group differences in p-cBF functional connectivity. A) Group differences between HC and MCI. MNI coordinates: X = 51, Y = -45, Z = 15. B) Group differences between HC and ADD. Upper row: MNI coordinates: X = -3, Y = 30, Z = 15. Lower row: MNI coordinates: X = 18, Y = -3, Z = -18. Two sample t-tests controlled for age, gender, years of education, and acquisition site. Colorbar indicates Cohen's d effect size values. Results are shown at an uncorrected voxel-wise threshold of $p < 0.001$ with a cluster-size threshold of $k > 10$ voxels.

p = 0.015; Cohen's d = 0.48) and ADD patients (+12.9 percent, p = 0.003; Cohen's d = 0.66) compared to HC, but was not significantly different from HC in the SCD group (+3.2 percent, p = 0.29; Cohen's d = 0.17).

3.5. Analysis with Aβ-stratified diagnostic groups

3.5.1. Effects of amyloid status in FC analysis

For the a-cBF, no significant differences in FC were observed in the HC^+ group when compared to the HC^- reference group. SCD^+ subjects showed one small cluster (14 voxels) of reduced connectivity in the right hippocampus and another cluster of 20 voxels in the left anterior cingulate. The MCI^+ group showed one cluster of reduced connectivity (21 voxels) in the right anterior cingulate, and the ADD^+ subgroup showed one larger cluster of reduced connectivity (175 voxels) in the left anterior cingulate (Fig. 5).

For the p-cBF, no significant differences in FC were observed in the HC^+ group when compared to the HC^- reference group. The SCD^+ group showed reduced connectivity in a small cluster in the left olfactory area (10 voxels), and the MCI^+ group presented a larger cluster of 174 voxels spanning the left caudate nucleus and the bilateral olfactory area. Similarly, the ADD^+ group showed a cluster of reduced connectivity (61 voxels) in the left nucleus caudatus and the bilateral olfactory area (Fig. 6).

3.5.2. Effects of amyloid status in volume analysis

There was a significant overall effect of group on both a-cBF (F = 3.52, $p < 0.001$) and p-cBF (F = 5.68, $p < 0.001$) volume (Fig. 7**A**). Comparing the amyloid positive subgroups to the HC^--group, a-cBF volume was significantly smaller in MCI^+ (-5.5 percent, p = 0.03; Cohen's d = -0.52) and ADD^+ (-11 percent, $p < 0.001$; Cohen's d = -1.04), but not in the SCD^+ (-0.9 percent, p = 0.71; Cohen's d = -0.09) or HC^+ (+2.3 percent, p = 0.43; Cohen's d = 0.21) groups. Similarly, in the p-cBF, volume was significantly smaller in MCI^+ (-7.4 percent, p = 0.003; Cohen's d = -0.73) and ADD^+ patients (-16.9 percent, $p < 0.001$; Cohen's d = -1.66), but not in the SCD^+ (-2.5 percent, p = 0.33; Cohen's d = -0.24) or HC^+ (+0.9 percent, p = 0.71; Cohen's d = 0.09) groups when compared to the HC^- group.

3.5.3. Effects of amyloid status in MD analysis

There was a significant overall effect of diagnosis on a-cBF MD (F = 2.25, p = 0.019) (Fig. 7**B**), although none of the pair-wise comparisons with the HC^- group reached statistical significance in the reduced subgroups (HC^+: +1.7 percent, p = 0.84, Cohen's d = 0.08; SCD^+: +9.9 percent, p = 0.20, Cohen's d = 0.44; MCI^+: +12.3 percent, p = 0.11, Cohen's d = 0.54; ADD^+: +11.6 percent, p = 0.20, Cohen's d = 0.52). There was no significant overall effect of diagnosis on p-cBF MD (F = 1.51, p = 0.14) (Fig. 7**B**).

4. Discussion

We studied cBF FC as measured by rs-fMRI as a possible indicator of early neurodegenerative processes in preclinical stages of AD. For comparison, we analysed established volumetric as well as DTI-based microstructural indices of cBF degeneration within a relatively large multicentric cohort study. Even though we were able to closely reproduce the previously reported FC profiles for the a-cBF and p-cBF functional subdivisions in this clinical sample, there were only minimal differences in FC between diagnostic groups. The analysis of volume and MD showed the expected differences in MCI and ADD patients when compared to the HC group, but no significant differences in the SCD group. These results remained largely unchanged when patient groups were limited to individuals with biomarker-confirmed Aβ-pathology.

4.1. FC profiles by seed region

The results from the FC analysis of a-cBF and p-cBF seeds were largely consistent with results from our previous study outlining the rs-fMRI based division of the cBF into anterior and posterior parts in healthy subjects spanning the adult age range (Fritz et al., 2019). Our results expand these findings by including subjects from the preclinical and clinical AD spectrum. In line with the previous study in healthy people (Fritz et al., 2019) and a study analysing FC of these cBF subdivisions in a group of subjects with subjective memory complaints (Chiesa et al., 2018), the FC of the a-cBF was characterized by connectivity to the ventromedial prefrontal cortex and the retrosplenial/posterior cingulate cortex. The p-cBF FC was characterized by connectivity to the Insula, the dACC, as well as the Thalamus. Thus, our study supports the subdivision of the cBF into two functionally segregated regions that are also in line with previous histological findings of distinct cortical projection patterns among cBF subdivisions (Mesulam et al., 1983).

4.2. FC differences between groups

Different to our a priori expectation, we found no significant voxel-

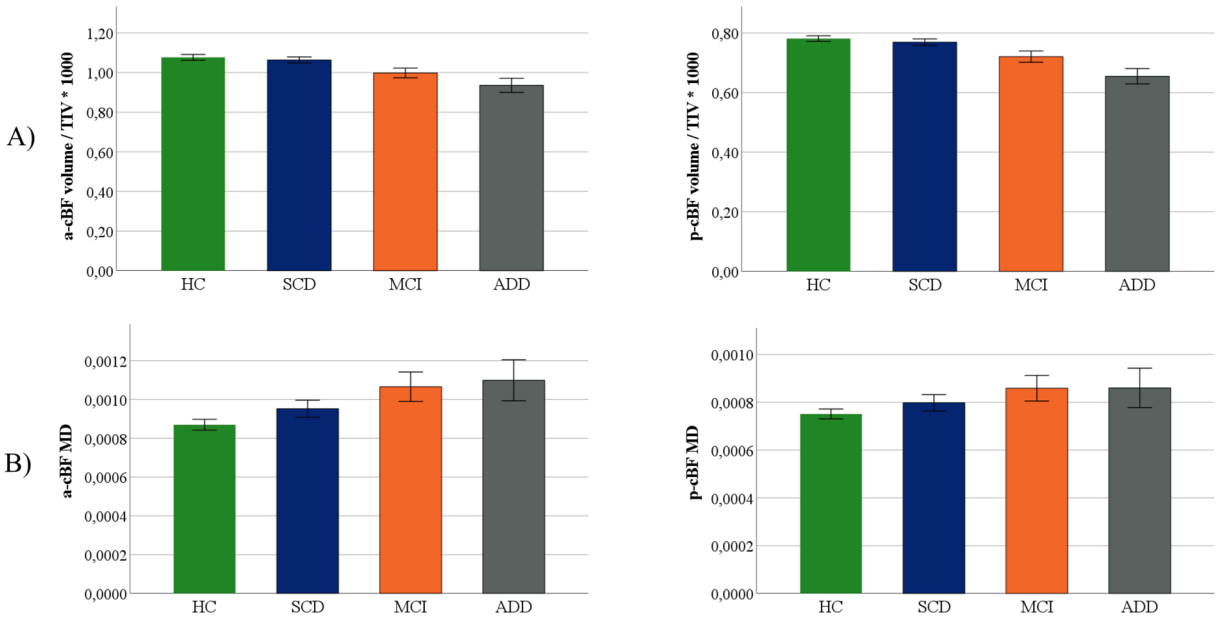

Fig. 4. Group differences in a-cBF and p-cBF volume and MD. Subregional volumes (A), and MD (B) for HC, SCD, MCI and ADD groups. Volume was normalized with total intracranial volume (TIV). Displayed are group wise means and standard errors of TIV-normalized volumes and MD.

wise differences in FC between the SCD and HC group even at a relatively lenient statistical threshold of $p < 0.001$, uncorrected.

Even though we found between group differences in the comparison of HC and the other diagnostic groups (MCI, ADD) as well as in the amyloid stratified comparison to HC^{-} (SCD^{+}, MCI^{+}, ADD^{+}), none of these results would have survived the application of stricter levels of significance entailed by appropriate multiple comparison corrections. While Cohen's d maps of the voxel-wise group differences in cBF-FC indicate peak effect sizes that are in a similar range as for the volumetric and diffusion analyses, it is important to note that these Cohen's d values are strongly positively biased because the voxel-wise analysis exploratively searches the largest group differences among all voxels of the respective FC profile. Therefore, these voxel-wise Cohen's d values reflect the largest possible effect size obtainable for FC analyses of the cBF seeds in this particular sample, and cannot be directly compared to the Cohen's d effect sizes obtained for the a priori ROI-based results of volume and MD changes in the cBF.

Our results are in contrast to a study examining FC of the NBM in a group of MCI patients that found a small cluster (87 voxels) of decreased connectivity in the left insula/claustrum (Li et al., 2017), which was cluster level corrected at $p < 0.05$. However, similar to our present findings the statistics indicated a relatively small effect size for this cluster. Furthermore, Li et al. used a stereotactic NBM ROI as seed region which forms a subset of our functionally-defined cBF seeds, and thus differences in the seed regions may have contributed to varying FC profiles.

Results from a previous study investigating FC of the cBF in a group with subjective memory complaints had indicated associations between p-cBF FC and global cortical amyloid load (Chiesa et al., 2018). By contrast, in our study we could not find robust effects of FC changes in amyloid positive SCD subjects compared with amyloid negative controls that would survive a corrected significance threshold. Apart from the smaller number of amyloid stratified cases in our study, one major difference is the derivation of amyloid status from CSF Aβ levels in our and from amyloid PET data in the previous study (Chiesa et al., 2018).

Considering rs-fMRI studies in participants with SCD in general, it is important to note that there is still no precise understanding of the type of disruption caused in SCD. There have been studies suggesting both reduced as well as increased FC in SCD (Hafkemeijer et al., 2013; López-Sanz et al., 2017), which likely reflects the large underlying pathological heterogeneity in SCD groups. Our findings of only small FC differences in SCD and MCI are in line with a previous study that was based on a partly overlapping sample from the DELCODE cohort (Teipel et al., 2018). In this study, the degree of diagnostic accuracy of whole brain FC analysis exceeded random guessing accuracy only in ADD, but not in MCI or SCD groups, suggesting little discriminatory power and possibly indicating a high level of noise in the functional data impeding the detection of differences (Teipel et al., 2018). Another possible explanation for the high consistency of FC across diagnostic groups could be an inherent resistance to reduction of FC that would be in line with findings of up-regulated choline acetyltransferase markers as a possible response to the onset of neurodegeneration found in neuropathological studies in MCI (Dekosky et al., 2002; Gilmor et al., 1999). However, cBF FC changes were even relatively small in the sample of ADD patients, for which cholinergic depletion is well established by both long-standing neuropathological as well as more recent neuroimaging studies (Bohnen et al., 2018). This suggests that cBF FC in rs-fMRI data may not represent a close imaging proxy of cortical cholinergic depletion.

4.3. Volume analyses

In accordance with our initial hypothesis, we found robust changes in cBF volume and MD in the MCI and ADD groups compared to controls. Previous MRI studies have mainly focussed on volume loss in the hippocampus, which has been shown to reliably differentiate the MCI stage (Jack et al., 2000, 1999; Pennanen et al., 2004). Studies on the cBF have yielded similar results in MCI (Kilimann et al., 2014; Muth et al., 2010). Furthermore, volumetric analysis of the cBF has been reported to be more sensitive to early degenerative changes in prodromal AD than hippocampal volume (Kilimann et al., 2014; Schmitz et al., 2016; Teipel et al., 2014a). Interestingly, previous neuropathological (Liu et al., 2015) and structural MRI studies (Kilimann et al., 2014; Teipel et al., 2014a) had specifically implicated the posterior subdivision of the NBM (Ch4p) in early and most pronounced neurodegeneration in AD. This was also supported by a study using volumetry of a cytoarchitectonically-defined posterior NBM subdivision of the cBF in an independent sample of SCD subjects (Scheef et al., 2019). Correspondingly, in our present analysis we observed consistently higher effect sizes for differences in p-cBF volumes compared to a-cBF volumes for all assessed group contrasts. However, even for p-cBF volumes the

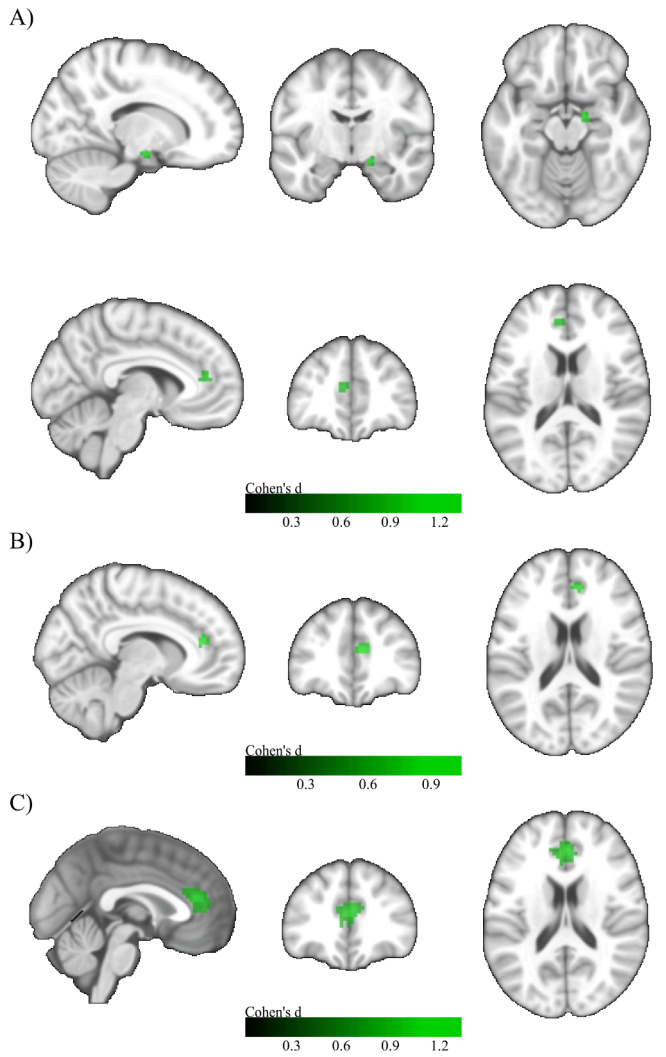

Fig. 5. Voxel-wise group differences in a-cBF functional connectivity in the amyloid stratified subgroups. A) Group differences between HC– and SCD + . Upper row: MNI coordinates: X = 15, Y = -9, Z = -15; Lower row: MNI coordinates: X = -6, Y = 42, Z = 15. B) Group differences between HC– and MCI + . MNI coordinates: X = 9, Y = 39, Z = 18. C) Group differences between HC– and ADD + . MNI coordinates: X = 0, Y = 36, Z = 18. Two sample t-tests controlled for age, gender, years of education, and acquisition site. Colorbar indicates Cohen's d effect size values. Results are shown at an uncorrected voxel-wise threshold of $p < 0.001$ with a cluster-size threshold of $k > 10$ voxels.

effect sizes were not large enough to yield significant volume reductions in the SCD or SCD^+ groups. This may at least partly be due to the fact that we focussed our analyses on two broader defined functional cBF subdivisions that are robustly differentiated by their different FC profiles in rs-fMRI data. One may hypothesize that volumetric analysis of the subtle changes at the SCD stage may be particularly susceptible to the exact part of the cBF that is being analysed and that larger ROIs may thus be less sensitive for the detection of these effects.

In the analysis of amyloid stratified subgroups, our results are in accordance with previous studies reporting significant volume loss in MCI^+ and ADD^+ (Grothe et al., 2014; Kerbler et al., 2015; Teipel et al., 2014a). Previous combined volumetric and amyloid-PET studies in MCI (Grothe et al., 2014; Kerbler et al., 2015; Teipel et al., 2014a) had suggested that cBF volumetry was strongly associated to amyloid burden and this was recently supported by evidence from an imaging-neuropathological association study (Teipel et al., 2020). Therefore, we had expected a stronger connection of cBF volume to amyloid status even in preclinical cases.

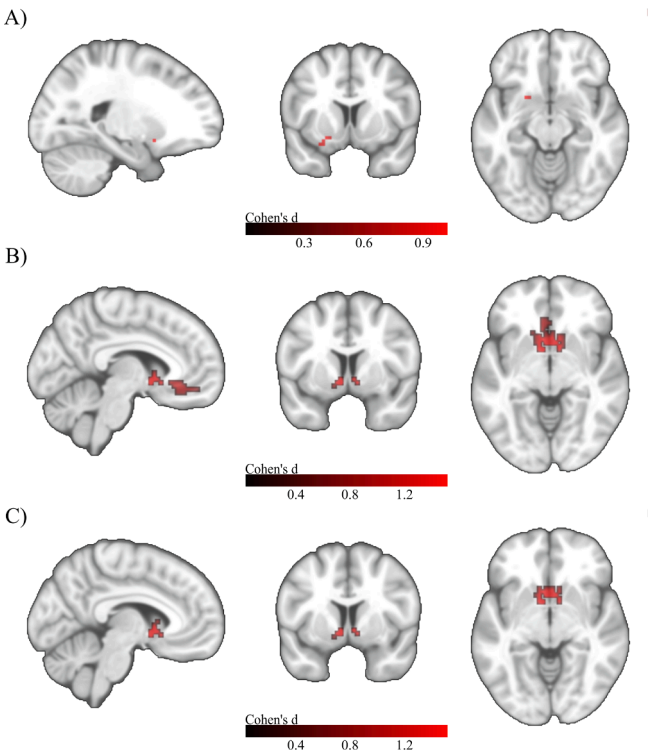

Fig. 6. Voxel-wise group differences in p-cBF functional connectivity in the amyloid stratified subgroups. A) Group differences between HC– and SCD + . MNI coordinates: X = -21, Y = 9, Z = -12. B) Group differences between HC– and MCI + . MNI coordinates: X = -6, Y = 6, Z = -6. C) Group differences between HC– and ADD + . MNI coordinates: X = -6, Y = 6, Z = -6. Two sample t-tests controlled for age, gender, years of education, and acquisition site. Colorbar indicates Cohen's d effect size values. Results are shown at an uncorrected voxel-wise threshold of $p < 0.001$ with a cluster-size threshold of $k > 10$ voxels.

4.4. MD analyses

MD was significantly increased in MCI and ADD patients when compared to HC. A previous study showed that MD in the cBF was predictive of progression from MCI to AD (Brueggen et al., 2015). However, similar to our current cross-sectional findings of comparable effect sizes for MD and volume differences, MD changes were not superior to volumetric measurements as predictors of conversion in that longitudinal follow-up study (Brueggen et al., 2015).

Similarly, another previous study suggested that MD was not a better marker than volume for detecting hippocampal degeneration in MCI (Henf et al., 2018). However, in contrast to these results, other studies suggested that analysis of hippocampal MD may be more sensitive than volumetric analysis in detecting subtle changes in pre-AD stages (Müller et al., 2007; Ryu et al., 2017).

Our study does not support the idea that in the absence of macrostructural cBF changes in very early stages of the AD spectrum microstructural cBF changes may instead be detected by analysis of MD. Two recent studies analysed WM MD in a partly overlapping sample from the DELCODE study. They also found only subtle (Brueggen et al., 2019) or no differences (Teipel et al., 2019) between HC and SCD subjects and concluded that WM MD may not be a useful biomarker for preclinical AD. The results from the present study extend these observations to MD of the cBF.

5. Limitations

This study has several limitations. First, even with standardized acquisition protocols and image quality control, between-group

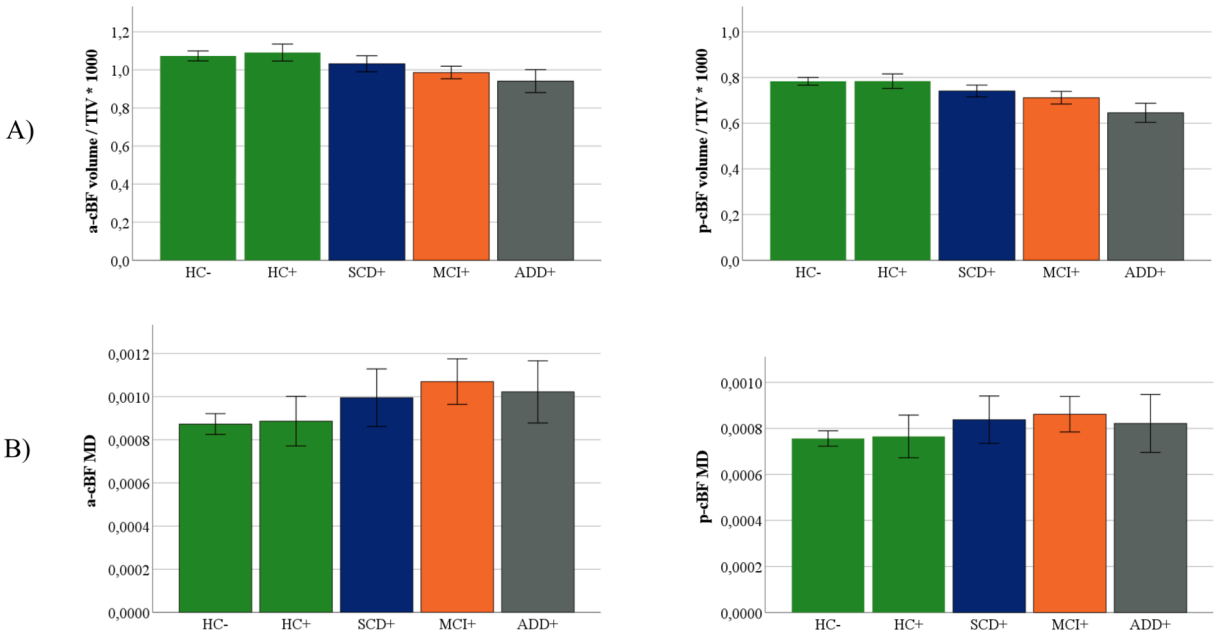

Fig. 7. Group differences in a-cBF and p-cBF volume and MD in the amyloid-stratified subgroups. Subregional volumes (A), and MD (B) for diagnostic groups stratified by amyloid status as determined by the CSF Aβ42/40-ratio. Volume was normalized with total intracranial volume (TIV). Displayed are the group wise means and standard errors of TIV-normalized volumes and MD.

differences, especially in the analysis of DTI data, may still be affected by inter-scanner variance (Teipel et al., 2019). However, a multicentric design is necessary for evaluating the robustness of group effects as a key requirement of potential imaging markers that are to be used in wider clinical settings. Furthermore, we did not assess a possible influence of partial volume effects on our results. The cBF is in relatively close vicinity to the CSF space, which could have contributed to a contamination of the cBF signal, particularly considering the relatively lower spatial resolution of rs-fMRI and DTI data (Gonzalez-Escamilla et al., 2017; Henf et al., 2018). However, it has to be noted that the cBF ROIs employed in our study were specifically defined on the basis of providing consistent FC signal in an independent rs-fMRI data set with comparable spatial resolution (Fritz et al., 2019). The observed FC profiles of the cBF subdivisions in our study were also highly comparable to the previously identified profiles (Fritz et al., 2019) and were reproducible across diagnostic groups, thus arguing against a major CSF signal confound in the employed cBF seeds. Moreover, at least for DTI-MD values a signal confound with CSF would generally lead to increased values, and thus these partial volume effects typically increase disease-related signal changes in neurodegenerative diseases (Henf et al., 2018). Therefore, in clinical contexts where the principal aim of an imaging biomarker is early detection of neurodegenerative disease, rather than the precise nature of the underlying tissue changes per se, eliminating these effects by partial volume correction methods may underestimate the diagnostic value of the imaging biomarker (Gonzalez-Escamilla et al., 2017).

The cross-sectional design of this study poses another limitation. For future research efforts, especially in the SCD group, longitudinal study designs will be invaluable as our current study is not able to differentiate between SCD participants who actually convert to ADD and those who remain stable over time. Longitudinal acquisition is currently ongoing in the DELCODE study which will allow studying the prognostic potential of the different imaging markers.

5.1. Conclusion

Overall these data indicate that neither cBF FC nor MD were superior to standard volumetric assessment in identifying early disease stages of AD. Future research in longitudinally characterized SCD samples may help to further elucidate the role of cBF changes in the development of AD and to assess the utility of multimodal MRI-derived measurements as predictive imaging biomarkers.

CRediT authorship contribution statement

Meret Herdick: Formal analysis, Investigation, Writing - original draft. **Martin Dyrba:** Data curation, Software, Methodology, Writing - review & editing. **Hans-Christian J. Fritz:** Software, Methodology, Writing - review & editing. **Slawek Altenstein:** Resources, Writing - review & editing. **Tommaso Ballarini:** Resources, Writing - review & editing. **Frederic Brosseron:** Resources, Writing - review & editing. **Katharina Buerger:** Resources, Writing - review & editing. **Arda Can Cetindag:** Resources, Writing - review & editing. **Peter Dechent:** Resources, Writing - review & editing. **Laura Dobisch:** Resources, Writing - review & editing. **Emrah Duezel:** Resources, Writing - review & editing. **Birgit Ertl-Wagner:** Resources, Writing - review & editing. **Klaus Fliessbach:** Resources, Writing - review & editing. **Silka Dawn Freiesleben:** Resources, Writing - review & editing. **Ingo Frommann:** Resources, Writing - review & editing. **Wenzel Glanz:** Resources, Writing - review & editing. **John Dylan Haynes:** Resources, Writing - review & editing. **Michael T. Heneka:** Resources, Writing - review & editing. **Daniel Janowitz:** Resources, Writing - review & editing. **Ingo Kilimann:** Resources, Writing - review & editing. **Christoph Laske:** Resources, Writing - review & editing. **Coraline D. Metzger:** Resources, Writing - review & editing. **Matthias H. Munk:** Resources, Writing - review & editing. **Oliver Peters:** Resources, Writing - review & editing. **Josef Priller:** Resources, Writing - review & editing. **Nina Roy:** Data curation, Resources, Writing - review & editing. **Klaus Scheffler:** Resources, Writing - review & editing. **Anja Schneider:** Resources, Writing - review & editing. **Annika Spottke:** Resources, Writing - review & editing. **Eike Jakob Spruth:** Resources, Writing - review & editing. **Maike Tscheuschler:** Resources, Writing - review & editing. **Ruth Vukovich:** Resources, Writing - review & editing. **Jens Wiltfang:** Resources, Writing - review & editing. **Frank Jessen:** Resources, Writing - review & editing. **Stefan Teipel:** Supervision, Resources, Writing - review & editing. **Michel J. Grothe:** Conceptualization, Methodology,

Supervision, Writing - original draft.

Declaration of Competing Interest

The authors declare that they have no known competing financial interests or personal relationships that could have appeared to influence the work reported in this paper.

Acknowledgements

Michel J. Grothe is supported by the "Miguel Servet" program [CP19/00031] of the Spanish Instituto de Salud Carlos III (ISCIII-FEDER).

DELCODE study group: S. Altenstein, H. Amthauer, A. Bader, M. Barkhoff, M. Beuth, H. Boecker, F. Brosseron, K. Brüggen, M. Buchmann, K. Bürger, C. Catak, L. Coloma Andrews, M. Daamen, S. de Jonge, M. Dichgans, A. Dörr, M. Dyrba, M. Ehrlich, T. Engels, B. Ertl-Wagner, C. Escher, J. Faber, K. Fliessbach, D. Frimmer, I. Frommann, M. Fuentes, N. Roshan Ghiasi, D. Hauser, T. Heger, C. Heine, J. Henf, G. Hennes, G. Herrmann, P. Hinderer, B. Huber, A. Hufen, H. Janecek-Meyer, D. Janowitz, F. Jessen, K. Kafali, C. Kainz, P. Kalbhen, E. Kasper, I. Kilimann, X. Kobeleva, B. Kofler, C. Korp, M. Kreuzer, E. Kuder-Buletta, C. Kurz, A. Langenfurth, C. Laske, E. Lau, K. Lindner, A. Lohse, H. Lützerath, F. Maier, E. Markov, B. Marquardt, A. Martikke, H. Megges, D. Meiberth, F. Menne, L. Miebach, A. Müller, C. Müller, C. Mychajliw, O. Peters, H. Pfaff, A. Polcher, J. Priller, H. Raum, A. Rominger, S. Röske, A. Rostamzadeh, P. Sabik, Y. Sagik, P. Sänger, L. Sannemann, A. Schild, J. Schmid (ehemals Spreider), M. Schmidt, C. Schneider, A. Schneider, H. Schulz, S. Schwarzenboeck, A. Seegerer, S. Sorgalla, A. Spottke, E. J. Spruth, J. Stephan, A. Szagarus, S. Teipel, M. Thelen, M. Tscheuschler, I. Villar Munoz, I. Vogt, M. Wagner, M. Weber, S. Weschke, C. Westerteicher, C. Widmann, S. Wolfsgruber, A. Zollver.

References

Albert, M.S., DeKosky, S.T., Dickson, D., Dubois, B., Feldman, H.H., Fox, N.C., Gamst, A., Holtzman, D.M., Jagust, W.J., Petersen, R.C., Snyder, P.J., Carrillo, M.C., Thies, B., Phelps, C.H., 2011. The diagnosis of mild cognitive impairment due to Alzheimer's disease: Recommendations from the National Institute on Aging-Alzheimer's Association workgroups on diagnostic guidelines for Alzheimer's disease. Alzheim. Demen. 7 (3), 270–279. https://doi.org/10.1016/j.jalz.2011.03.008.

Ashburner, J., 2007. A fast diffeomorphic image registration algorithm. NeuroImage 38 (1), 95–113. https://doi.org/10.1016/j.neuroimage.2007.07.007.

Basser, P.J., Mattiello, J., Lebihan, D., 1994. Estimation of the Effective Self-Diffusion Tensor from the NMR Spin Echo. J. Magn. Reson., Ser B 103 (3), 247–254. https://doi.org/10.1006/jmrb.1994.1037.

Biswal, B., Zerrin Yetkin, F., Haughton, V.M., Hyde, J.S., 1995. Functional connectivity in the motor cortex of resting human brain using echo-planar mri. Magn. Reson. Med. 34 (4), 537–541. https://doi.org/10.1002/mrm.1910340409.

Bohnen, N.I., Grothe, M.J., Ray, N.J., Müller, M.L.T.M., Teipel, S.J., 2018. Recent Advances in Cholinergic Imaging and Cognitive Decline—Revisiting the Cholinergic Hypothesis of Dementia. Curr Geri Rep 7 (1), 1–11. https://doi.org/10.1007/s13670-018-0234-4.

Brueggen, K., Dyrba, M., Barkhof, F., Hausner, L., Filippi, M., Nestor, P.J., Hauenstein, K., Klöppel, S., Grothe, M.J., Kasper, E., Teipel, S.J., 2015. Basal Forebrain and Hippocampus as Predictors of Conversion to Alzheimer's Disease in Patients with Mild Cognitive Impairment – A Multicenter DTI and Volumetry Study. JAD 48 (1), 197–204. https://doi.org/10.3233/JAD-150063.

Brueggen, K., Dyrba, M., Cardenas-Blanco, A., Schneider, A., Fliessbach, K., Buerger, K., Janowitz, D., Peters, O., Menne, F., Priller, J., Spruth, E., Wiltfang, J., Vukovich, R., Laske, C., Buchmann, M., Wagner, M., Röske, S., Spottke, A., Rudolph, J., Metzger, C. D., Kilimann, I., Dobisch, L., Düzel, E., Jessen, F., Teipel, S.J., 2019. Structural integrity in subjective cognitive decline, mild cognitive impairment and Alzheimer's disease based on multicenter diffusion tensor imaging. J. Neurol. 266 (10), 2465–2474. https://doi.org/10.1007/s00415-019-09429-3.

Chiesa, P.A., Cavedo, E., Grothe, M.J., Houot, M., Teipel, S.J., Potier, M.-C., Habert, M.-O., Lista, S., Dubois, B., Hampel, H., 2018. Relationship between Basal Forebrain Resting-State Functional Connectivity and Brain Amyloid-β Deposition in Cognitively Intact Older Adults with Subjective Memory Complaints. Radiology 290 (1), 167–176. https://doi.org/10.1148/radiol.2018180268.

DeKosky, S.T., Ikonomovic, M.D., Styren, S.D., Beckett, L., Wisniewski, S., Bennett, D.A., Cochran, E.J., Kordower, J.H., Mufson, E.J., 2002. Upregulation of choline acetyltransferase activity in hippocampus and frontal cortex of elderly subjects with mild cognitive impairment. Ann. Neurol. 51 (2), 145–155. https://doi.org/10.1002/ana.10069.

Friston, K.J., Williams, S., Howard, R., Frackowiak, R.S.J., Turner, R., 1996. Movement-Related effects in fMRI time-series: Movement Artifacts in fMRI. Magn. Reson. Med. 35 (3), 346–355. https://doi.org/10.1002/mrm.1910350312.

Fritz, H.-C., Ray, N., Dyrba, M., Sorg, C., Teipel, S., Grothe, M.J., 2019. The corticotopic organization of the human basal forebrain as revealed by regionally selective functional connectivity profiles. Hum. Brain Mapp. 40 (3), 868–878. https://doi.org/10.1002/hbm.24417.

Gilmor, M.L., Erickson, J.D., Varoqui, H., Hersh, L.B., Bennett, D.A., Cochran, E.J., Mufson, E.J., Levey, A.I., 1999. Preservation of nucleus basalis neurons containing choline acetyltransferase and the vesicular acetylcholine transporter in the elderly with mild cognitive impairment and early Alzheimer's disease. J. Comp. Neurol. 411, 693–704. https://doi.org/10.1002/(SICI)1096-9861(19990906)411:4<693::AID-CNE13>3.0.CO;2-D.

Glover, G.H., 2011. Overview of Functional Magnetic Resonance Imaging. Neurosurg. Clin. N. Am. 22 (2), 133–139. https://doi.org/10.1016/j.nec.2010.11.001.

Gonzalez-Escamilla, G., Lange, C., Teipel, S., Buchert, R., Grothe, M.J., 2017. PETPVE12: an SPM toolbox for Partial Volume Effects correction in brain PET – Application to amyloid imaging with AV45-PET. NeuroImage 147, 669–677. https://doi.org/10.1016/j.neuroimage.2016.12.077.

Grothe, M., Heinsen, H., Teipel, S.J., 2012. Atrophy of the Cholinergic Basal Forebrain Over the Adult Age Range and in Early Stages of Alzheimer's Disease. Biol. Psychiatry 71 (9), 805–813. https://doi.org/10.1016/j.biopsych.2011.06.019.

Grothe, M.J., Ewers, M., Krause, B., Heinsen, H., Teipel, S.J., 2014. Basal forebrain atrophy and cortical amyloid deposition in nondemented elderly subjects. Alzheimer's & Dementia 10, S344–S353. https://doi.org/10.1016/j.jalz.2013.09.011.

Hafkemeijer, A., Altmann-Schneider, I., Oleksik, A.M., van de Wiel, L., Middelkoop, H.A. M., van Buchem, M.A., van der Grond, J., Rombouts, S.A.R.B., 2013. Increased Functional Connectivity and Brain Atrophy in Elderly with Subjective Memory Complaints. Brain Connect. 3 (4), 353–362. https://doi.org/10.1089/brain.2013.0144.

Henf, J., Grothe, M.J., Brueggen, K., Teipel, S., Dyrba, M., 2018. Mean diffusivity in cortical gray matter in Alzheimer's disease: The importance of partial volume correction. NeuroImage: Clinical 17, 579–586. https://doi.org/10.1016/j.nicl.2017.10.005.

Hong, Y.J., Yoon, B., Lim, S.-C., Shim, Y.S., Kim, J.-Y., Ahn, K.J., Han, I.-W., Yang, D.W., 2012. Microstructural changes in the hippocampus and posterior cingulate in mild cognitive impairment and Alzheimer's disease: a diffusion tensor imaging study. Neurol Sci 34 (7), 1215–1221. https://doi.org/10.1007/s10072-012-1225-4.

Jack, C.R., Petersen, R.C., Xu, Y., O'Brien, P.C., Smith, G.E., Ivnik, R.J., Boeve, B.F., Tangalos, E.G., Kokmen, E., 2000. Rates of hippocampal atrophy correlate with change in clinical status in aging and AD. Neurology 55 (4), 484–490. https://doi.org/10.1212/WNL.55.4.484.

Jack, C.R., Petersen, R.C., Xu, Y.C., O'Brien, P.C., Smith, G.E., Ivnik, R.J., Boeve, B.F., Waring, S.C., Tangalos, E.G., Kokmen, E., 1999. Prediction of AD with MRI-based hippocampal volume in mild cognitive impairment. Neurology 52 (7), 1397. https://doi.org/10.1212/WNL.52.7.1397.

Janelidze, S., Zetterberg, H., Mattsson, N., Palmqvist, S., Vanderstichele, H., Lindberg, O., van Westen, D., Stomrud, E., Minthon, L., Blennow, K., Hansson, O., 2016. CSF A42/A40 and A42/A38 ratios: better diagnostic markers of Alzheimer disease. Ann. Clin. Transl. Neurol. 3, 154–165. https://doi.org/10.1002/acn3.274.

Jessen, F., Amariglio, R.E., van Boxtel, M., Breteler, M., Ceccaldi, M., Chételat, G., Dubois, B., Dufouil, C., Ellis, K.A., van der Flier, W.M., Glodzik, L., van Harten, A.C., de Leon, M.J., McHugh, P., Mielke, M.M., Molinuevo, J.L., Mosconi, L., Osorio, R.S., Perrotin, A., Petersen, R.C., Rabin, L.A., Rami, L., Reisberg, B., Rentz, D.M., Sachdev, P.S., de la Sayette, V., Saykin, A.J., Scheltens, P., Shulman, M.B., Slavin, M. J., Sperling, R.A., Stewart, R., Uspenskaya, O., Vellas, B., Visser, P.J., Wagner, M., 2014. A conceptual framework for research on subjective cognitive decline in preclinical Alzheimer's disease. Alzheim. Dementia 10 (6), 844–852. https://doi.org/10.1016/j.jalz.2014.01.001.

Jessen, F., Spottke, A., Boecker, H., Brosseron, F., Buerger, K., Catak, C., Fliessbach, K., Franke, C., Fuentes, M., Heneka, M.T., Janowitz, D., Kilimann, I., Laske, C., Menne, F., Nestor, P., Peters, O., Priller, J., Pross, V., Ramirez, A., Schneider, A., Speck, O., Spruth, E.J., Teipel, S., Vukovich, R., Westerteicher, C., Wiltfang, J., Wolfsgruber, S., Wagner, M., Düzel, E., 2018. Design and first baseline data of the DZNE multicenter observational study on predementia Alzheimer's disease (DELCODE). Alz. Res. Therapy 10 (1). https://doi.org/10.1186/s13195-017-0314-2.

Joel, S.E., Caffo, B.S., van Zijl, P.C.M., Pekar, J.J., 2011. On the relationship between seed-based and ICA-based measures of functional connectivity: Relationship Between Seed-Based and ICA Connectivity. Magn. Reson. Med. 66 (3), 644–657. https://doi.org/10.1002/mrm.22818.

Kerbler, G.M., Fripp, J., Rowe, C.C., Villemagne, V.L., Salvado, O., Rose, S., Coulson, E.J., 2015. Basal forebrain atrophy correlates with amyloid β burden in Alzheimer's disease. NeuroImage: Clinical 7, 105–113. https://doi.org/10.1016/j.nicl.2014.11.015.

Kilimann, I., Grothe, M., Heinsen, H., Alho, E.J.L., Grinberg, L., Amaro Jr., E., dos Santos, G.A.B., da Silva, R.E., Mitchell, A.J., Frisoni, G.B., Bokde, A.L.W., Fellgiebel, A., Filippi, M., Hampel, H., Klöppel, S., Teipel, S.J., 2014. Subregional Basal Forebrain Atrophy in Alzheimer's Disease: A Multicenter Study. JAD 40 (3), 687–700. https://doi.org/10.3233/JAD-132345.

Li, H., Jia, X., Qi, Z., Fan, X., Ma, T., Ni, H., Li, C.R., Li, K., 2017. Altered Functional connectivity of the basal nucleus of meynert in mild cognitive impairment: a resting-state fMRI study. Front. Aging Neurosci. 9, 127. https://doi.org/https://doi.org/10.3389/fnagi.2017.00127.

Liu, A.K.L., Chang, R.-C., Pearce, R.K.B., Gentleman, S.M., 2015. Nucleus basalis of Meynert revisited: anatomy, history and differential involvement in Alzheimer's and

Parkinson's disease. Acta Neuropathol. 129 (4), 527–540. https://doi.org/10.1007/s00401-015-1392-5.

López-Sanz, D., Bruña, R., Garcés, P., Martín-Buro, M.C., Walter, S., Delgado, M.L., Montenegro, M., Higes, R.L., Marcos, A., Maestú, F., 2017. Functional Connectivity Disruption in Subjective Cognitive Decline and Mild Cognitive Impairment: A Common Pattern of Alterations. Front. Aging Neurosci. 9 https://doi.org/10.3389/fnagi.2017.00109.

McGeer, P.L., McGeer, E.G., Suzuki, J., Dolman, C.E., Nagai, T., 1984. Aging, Alzheimer's disease, and the cholinergic system of the basal forebrain. Neurology 34 (6), 741. https://doi.org/10.1212/WNL.34.6.741.

McKhann, G.M., Knopman, D.S., Chertkow, H., Hyman, B.T., Jack Jr., C.R., Kawas, C.H., Klunk, W.E., Koroshetz, W.J., Manly, J.J., Mayeux, R., Mohs, R.C., Morris, J.C., Rossor, M.N., Scheltens, P., Carrillo, M.C., Thies, B., Weintraub, S., Phelps, C.H., 2011. The diagnosis of dementia due to Alzheimer's disease: Recommendations from the National Institute on Aging-Alzheimer's Association workgroups on diagnostic guidelines for Alzheimer's disease. Alzheim. Demen. 7 (3), 263–269. https://doi.org/10.1016/j.jalz.2011.03.005.

Mesulam, M.-M., Mufson, E.J., Levey, A.I., Wainer, B.H., 1983. Cholinergic innervation of cortex by the basal forebrain: Cytochemistry and cortical connections of the septal area, diagonal band nuclei, nucleus basalis (Substantia innominata), and hypothalamus in the rhesus monkey. J. Comp. Neurol. 214 (2), 170–197. https://doi.org/10.1002/cne.902140206.

Müller, M.J., Greverus, D., Weibrich, C., Dellani, P.R., Scheurich, A., Stoeter, P., Fellgiebel, A., 2007. Diagnostic utility of hippocampal size and mean diffusivity in amnestic MCI. Neurobiol. Aging 28 (3), 398–403. https://doi.org/10.1016/j.neurobiolaging.2006.01.009.

Muth, K., Schönmeyer, R., Matura, S., Haenschel, C., Schröder, J., Pantel, J., 2010. Mild Cognitive Impairment in the Elderly is Associated with Volume Loss of the Cholinergic Basal Forebrain Region. Biol. Psychiatry 67 (6), 588–591. https://doi.org/10.1016/j.biopsych.2009.02.026.

Pennanen, C., Kivipelto, M., Tuomainen, S., Hartikainen, P., Hänninen, T., Laakso, M.P., Hallikainen, M., Vanhanen, M., Nissinen, A., Helkala, E.-L., Vainio, P., Vanninen, R., Partanen, K., Soininen, H., 2004. Hippocampus and entorhinal cortex in mild cognitive impairment and early AD. Neurobiol. Aging 25 (3), 303–310. https://doi.org/10.1016/S0197-4580(03)00084-8.

Ryu, S.Y., Lim, E.Y., Na, S., Shim, Y.S., Cho, J.H., Yoon, B., Hong, Y.J., Yang, D.W., 2017. Hippocampal and entorhinal structures in subjective memory impairment: a combined MRI volumetric and DTI study. Int. Psychogeriatr. 29 (5), 785–792. https://doi.org/10.1017/S1041610216002349.

Scheef, L., Grothe, M.J., Koppara, A., Daamen, M., Boecker, H., Biersack, H., Schild, H.H., Wagner, M., Teipel, S., Jessen, F., 2019. Subregional volume reduction of the cholinergic forebrain in subjective cognitive decline (SCD). NeuroImage: Clinical 21, 101612. https://doi.org/10.1016/j.nicl.2018.101612.

Schmitz, T.W., Spreng, R.N., Weiner, M.W., Aisen, P., Petersen, R., Jack, C.R., Jagust, W., Trojanowki, J.Q., Toga, A.W., Beckett, L., others, 2016. Basal forebrain degeneration precedes and predicts the cortical spread of Alzheimer's pathology. Nat. commun. 7, 13249. https://doi.org/https://doi.org/10.1038/ncomms13249.

Schulz, J., Pagano, G., Fernández Bonfante, J.A., Wilson, H., Politis, M., 2018. Nucleus basalis of Meynert degeneration precedes and predicts cognitive impairment in Parkinson's disease. Brain 141, 1501–1516. https://doi.org/https://doi.org/10.1093/brain/awy072.

Teipel, S., Heinsen, H., Amaro Jr., E., Grinberg, L.T., Krause, B., Grothe, M., 2014a. Cholinergic basal forebrain atrophy predicts amyloid burden in Alzheimer's disease. Neurobiol. Aging 35 (3), 482–491. https://doi.org/10.1016/j.neurobiolaging.2013.09.029.

Teipel, S.J., Fritz, H.-C., Grothe, M.J., 2020. Alzheimer's Disease Neuroimaging Initiative, others, Neuropathological features associated with basal forebrain atrophy in Alzheimer's disease. Neurology. https://doi.org/10.1212/WNL.0000000000010192.

Teipel, Stefan J., Kuper-Smith, Jan O., Bartels, Claudia, Brosseron, Frederic, Buchmann, Martina, Buerger, Katharina, Catak, Cihan, Janowitz, Daniel, Dechent, Peter, Dobisch, Laura, Ertl-Wagner, Birgit, Fließbach, Klaus, Haynes, John-Dylan, Heneka, Michael T., Kilimann, Ingo, Laske, Christoph, Li, Siyao, Menne, Felix, Metzger, Coraline D., Priller, Josef, Pross, Verena, Ramirez, Alfredo, Scheffler, Klaus, Schneider, Anja, Spottke, Annika, Spruth, Eike J., Wagner, Michael, Wiltfang, Jens, Wolfsgruber, Steffen, Düzel, Emrah, Jessen, Frank, Dyrba, Martin, Zhou, Juan Helen, 2019. Multicenter Tract-Based Analysis of Microstructural Lesions within the Alzheimer's Disease Spectrum: Association with Amyloid Pathology and Diagnostic Usefulness. JAD 72 (2), 455–465. https://doi.org/10.3233/JAD-190446.

Teipel, Stefan J., Metzger, Coraline D., Brosseron, Frederic, Buerger, Katharina, Brueggen, Katharina, Catak, Cihan, Diesing, Dominik, Dobisch, Laura, Fliebach, Klaus, Franke, Christiana, Heneka, Michael T., Kilimann, Ingo, Kofler, Barbara, Menne, Felix, Peters, Oliver, Polcher, Alexandra, Priller, Josef, Schneider, Anja, Spottke, Annika, Spruth, Eike J., Thelen, Manuela, Thyrian, René J., Wagner, Michael, Düzel, Emrah, Jessen, Frank, Dyrba, Martin, 2018. Multicenter Resting State Functional Connectivity in Prodromal and Dementia Stages of Alzheimer's Disease. JAD 64 (3), 801–813. https://doi.org/10.3233/JAD-180106.

Teipel, Stefan J., Reuter, Sigrid, Stieltjes, Bram, Acosta-Cabronero, Julio, Ernemann, Ulrike, Fellgiebel, Andreas, Filippi, Massimo, Frisoni, Giovanni, Hentschel, Frank, Jessen, Frank, Klöppel, Stefan, Meindl, Thomas, Pouwels, Petra J. W., Hauenstein, Karl-Heinz, Hampel, Harald, 2011. Multicenter stability of diffusion tensor imaging measures: A European clinical and physical phantom study. Psychiat. Res. Neuroimag. 194 (3), 363–371. https://doi.org/10.1016/j.pscychresns.2011.05.012.

Teipel, Stefan J., Walter, Martin, Likitjaroen, Yuttachai, Schönknecht, Peter, Gruber, Oliver, 2014b. Diffusion tensor imaging in Alzheimer's disease and affective disorders. Eur. Arch. Psychiatry Clin. Neurosci. 264 (6), 467–483. https://doi.org/10.1007/s00406-014-0496-6.

Uluğ, A.M., Moore, D.F., Bojko, A.S., Zimmerman, R.D., 1999. Clinical use of diffusion-tensor imaging for diseases causing neuronal and axonal damage. Am. J. Neuroradiol. 20, 1044–1048.

Wang, Liang, Zang, Yufeng, He, Yong, Liang, Meng, Zhang, Xinqing, Tian, Lixia, Wu, Tao, Jiang, Tianzi, Li, Kuncheng, 2006. Changes in hippocampal connectivity in the early stages of Alzheimer's disease: Evidence from resting state fMRI. NeuroImage 31 (2), 496–504. https://doi.org/10.1016/j.neuroimage.2005.12.033.

Whitehouse, Peter J., Price, Donald L., Clark, Arthur W., Coyle, Joseph T., DeLong, Mahlon R., 1981. Alzheimer disease: Evidence for selective loss of cholinergic neurons in the nucleus basalis. Ann. Neurol. 10 (2), 122–126. https://doi.org/10.1002/ana.410100203.

Whitehouse, P., Price, D., Struble, R., Clark, A., Coyle, J., Delon, M., 1982. Alzheimer's disease and senile dementia: loss of neurons in the basal forebrain. Science 215 (4537), 1237–1239. https://doi.org/10.1126/science:7058341.

Yan, C., Zang, Y., 2010. DPARSF: a MATLAB toolbox for" pipeline" data analysis of resting-state fMRI. Front. Syst. Neurosci. 4, 13. Doi: 10.3389/fnsys.2010.00013.

ZHANG, H, WANG, S, XING, J, LIU, B, MA, Z, YANG, M, ZHANG, Z, TENG, G, 2009. Detection of PCC functional connectivity characteristics in resting-state fMRI in mild Alzheimer's disease. Behav. Brain Res. 197 (1), 103–108. https://doi.org/10.1016/j.bbr.2008.08.012.

Zhou, Yongxia, Dougherty Jr, John H., Hubner, Karl F., Bai, Bing, Cannon, Rex L., Hutson, R. Kent, 2008. Abnormal connectivity in the posterior cingulate and hippocampus in early Alzheimer's disease and mild cognitive impairment. Alzheim. Demen. 4 (4), 265–270. https://doi.org/10.1016/j.jalz.2008.04.006.